JOURNAL OF SOLID STATE CHEMISTRY 95, 111–125 (1991)

Incommensurately Modulated $ZrO_{2-x}F_{2x}$: $0.698 \leq x \leq 0.714$

J. G. THOMPSON,* R. L. WITHERS

Research School of Chemistry, Australian National University, GPO Box 4 Canberra, ACT 2601, Australia

AND C. J. KEPERT

Chemistry Department, University of Western Australia, Nedlands, WA 6009, Australia

Received April 1, 1991

The compound $ZrO_{2-x}F_{2x}$ has been studied by X-ray powder diffraction and transmission electron microscopy. It was previously described as a series of anion-deficient, α-UO_3-type "line phases," with compositions in between resulting from unit cell scale intergrowths of the line phases. More correctly $ZrO_{2-x}F_{2x}$ is described as an incommensurately modulated structure with composition-dependent primary modulation wave-vector, $\mathbf{q} = x\mathbf{b}^*$. The underlying orthorhombically distorted α-UO_3-type parent structure has space group symmetry *Cmmm* ($a \approx 6.44$, $b \approx 3.83$, $c \approx 4.07$ Å). Characteristic extinction conditions imply a superspace group symmetry of $P:Cmmm:s,-1,1$. The previously reported crystal structure of $Zr_7O_9F_{10}$ is Fourier decomposed in these terms. Crystal chemical reasons are proposed for the very limited composition range, $0.698 \leq x \leq 0.714$, observed for the title compound.

1. Introduction

The system ZrO_2–ZrF_4 has been extensively studied previously by X-ray powder diffraction (*1–4*), transmission electron microscopy (*4, 5*), and single crystal X-ray diffraction (*6–8*). It has been reported that, at approximately 35 mole% ZrF_4, there exists a series of α-U_3O_8-type related compounds with stoichiometries $Zr_4O_5F_6$, $Zr_7O_9F_{10}$, and $Zr_{10}O_{13}F_{14}$ (*2*). The crystal structures of these compounds like that of α-U_3O_8 were understood to be superstructures of an orthorhombically distorted α-UO_3-type ($a \approx 6.44$, $b \approx 3.84$, $c \approx 4.09$ Å), with the superstructure resulting from the ordering of anion vacancies (v, $Zr(O, F)_{3-v}$) along the **b** direction. The crystal structure of the compound $Zr_7O_9F_{10}$ has been refined (*6*) and confirmed this understanding.

Ceramics in the ZrO_2–ZrF_4 system, which include the title compound, have been studied as a possible means of immobilizing the waste zircaloy nuclear fuel cladding produced during the reprocessing of spent fuel from water-cooled reactors (*9*).

Recent work by us on the system ZrO_2–Nb_2O_5 (*10*) showed that what was previously thought to be a homologous series of compounds M_nO_{2n+1}, with fluorite-related superstructures (*11*), was in fact an incom-

*To whom correspondence should be addressed.

0022-4596/91 $3.00

mensurately modulated, fluorite-related structure ($Nb_2Zr_{x-2}O_{2x+1}$: $7.1 \leq x \leq 10.3$) with primary modulation wave-vector ($\mathbf{q} = \mathbf{b}^* + \frac{1}{x}\mathbf{a}^*$) varying as a function of composition.

Early work on the title compound (*2*) suggested that it was a homologous series $Zr_{3n+1}O_{4n+1}F_{4n+2}$ ($n = 1, 2, 3$), while later work (*6*) preferred to described it as a series $(Zr(O, F))_{2(3n+1)}$ $(O, F)_{4(3n+1)-2n}$ where $2n$ represents the number of anions subtracted from the unit cell and $3n + 1$ the multiplicity of the **b** parameter. All in-between compositions were interpreted (*5, 6*) as unit cell scale intergrowths of the members of this series. A preliminary study of $Zr_7O_9O_{10}$ by TEM electron diffraction suggested that this previously reported homologous series might, in fact, actually be an incommensurately modulated α-UO_3-related structure with modulation wave-vector varying with composition, as for $Nb_2Zr_{x-2}O_{2x+1}$.

For this reason, we undertook a systematic study of the ZrO_2-rich end of the system ZrO_2–ZrF_4, i.e., $ZrO_{2-x}F_{2x}$, to test this hypothesis.

2. Experimental

2.1 Synthesis

Initial attempts to synthesize single phase $ZrO_{2-x}F_{2x}$ specimens at an accurately known composition proved very difficult, due to the air sensitivity of ZrF_4 and loss of ZrF_4 upon reaction above its sublimation temperature of ~600°C. It was decided to circumvent these difficulties by synthesizing in the two phase region on either side of the subject compound.

Specimens were prepared from "ZrO_2" (Z-Tech Pty. Ltd., >99.95% containing 2.57% HfO_2) and ZrF_4 (Cerac Inc., 99.9% pure) at compositions 30 and 50 mole% ZrF_4. Specimens at both compositions were mechanically mixed and heated for variable lengths of time at 600, 700, 800, 900, and 1000°C, in both sealed Pt tubes and in open (crimped) Pt tubes under 1 atm of oxygen-free nitrogen.

The duration of reaction varied from ~15 min at 1000°C to ~3 days at 600°C in order to reach equilibrium. Because of the comments made by Papiernik *et al.* (*4*) that the reaction product was very dependent on the conditions of synthesis, particularly at low temperature at the ZrF_4-rich end of the series, the two 600°C specimens in sealed Pt tubes were reground and heated for a further week at 600°C to confirm that equilibrium had in fact been reached. Also, in response to these comments, we chose to run parallel syntheses under quite different $p(ZrF_4)$ and $p(O_2)$ conditions.

2.2 XRD and Electron Diffraction

Specimens were examined by XRD using a Guinier–Hägg camera with monochromated Cu$K\alpha_1$ radiation. An internal standard of Si (NBS No. 640) was used to calibrate the measurement of XRD films for least-squares refinement of the unit cell dimensions and the magnitude of the modulation vector. The material was further studied on a JEOL 100CX transmission electron microscope.

3. Results and Discussion

3.1 Phase Relationships

The phase relationships are as reported by Papiernik *et al.* (*4*) except that the incommensurately modulated $ZrO_{2-x}F_{2x}$ ($0.698 \leq x \leq 0.714$) phase field is treated as a single "solid–solution." The compositions of the end-members of the solid–solution field are difficult to ascertain due to its narrow range. Correct interpretation of the magnitude of the primary modulation vector should, however, provide a means for determining composition. A discussion of the modulation vector will be given in Section 3.8.

In accord with the results of Papiernik and Frit (*5*) the fluorite-related phase mentioned

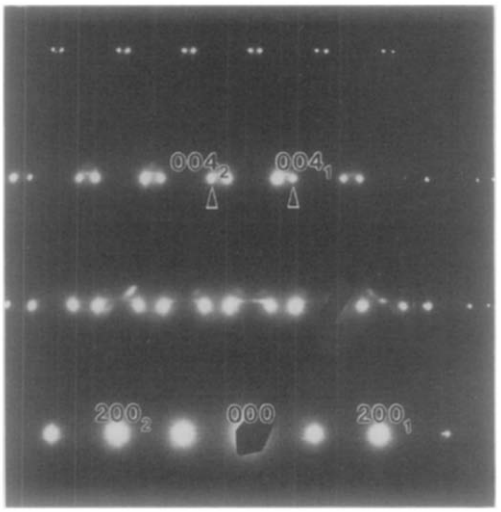

FIG. 1. An [010] zone axis SADP of baddeleyite (monoclinic ZrO_2) multiply twinned on (100). The two twin orientations are labeled with subscript 1 or 2.

by Joubert and Gaudreau (*2*) with composition ~4.2 mole% ZrF_4 was found not to exist. This supposed phase was almost certainly baddeleyite multiply twinned on (100). The twinned lattice can approximately be fitted by a six-times superstructure of an orthorhombic fluorite-related unit cell; as in baddeleyite the monoclinic angle β^* is very close to 80° and $a^* \approx c^*$ (*12*) (see Fig. 1). All the Guinier photographs of specimens prepared at 30 mole% ZrF_4 could be completely indexed as $ZrO_{2-x}F_{2x}$ and baddeleyite.

For the 50 mole% ZrF_4 specimens, the second phase present was hexagonal $Zr_3O_2F_8$ (*8*) up to and including 700°C, and ReO_3-type cubic $Zr_3O_2F_8$ above 700°C (*4*). The phase transition temperature reported by Papiernik *et al.* (*4*) was 710°C. No temperature dependence of their unit cell dimensions was evident, but hexagonal $Zr_3O_2F_8$ (space group $P6_3mc$, $a = 7.671$, $c = 12.49$ Å) showed a high density of planar faults perpendicular to the **c** direction (see Fig. 2a). The $\{-h, h, 0, l\}^*$ reflections in the corresponding ⟨110⟩ zone-axis SADPs (see Fig. 2b) were always heavily streaked along the **c*** direction unless $h = 3n$, suggesting that the planar faults are displacement faults with fault vector $\mathbf{R} = \frac{1}{3}\mathbf{a}, \frac{1}{3}\mathbf{b}$ or $\frac{1}{3}(\mathbf{a} + \mathbf{b})$.

3.2 Magnitude of the Modulation Vector

The magnitude of the modulation vector for these end member compositions was determined from both X-ray powder diffraction and electron diffraction patterns. The electron diffraction patterns showed that the

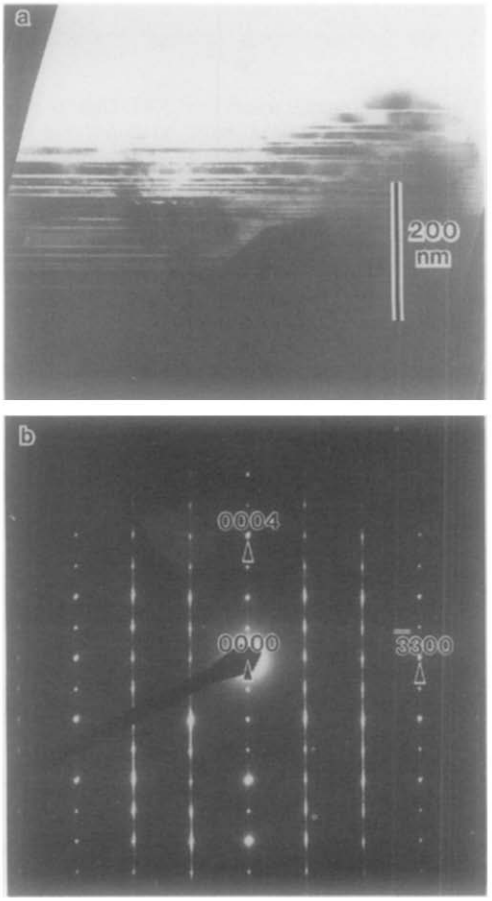

FIG. 2. A typical ⟨110⟩ bright field electron micrograph of hexagonal $Zr_3O_2F_8$ showing a high density of planar faults perpendicular to the **c** direction along with the corresponding SADP. Note the heavy streaking along **c*** of all $\{-h, h, 0, l\}^*$ reflections for which $h \neq 3n$, n an integer.

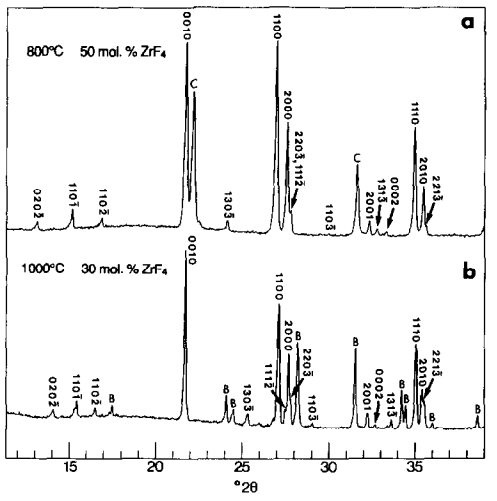

FIG. 3. Densitometer traces from XRD Guinier exposures (λ = 1.5406 Å) of (a) 800°C 50 mole% ZrF_4 and (b) 1000°C 30 mole% ZrF_4 specimens. The upper trace shows $x = 0.714$ in equilibrium with ReO_3-type cubic $Zr_3O_2F_8$ (labeled C) and the lower trace $x = 0.698$ and baddeleyite (labeled B). A four-index notation (h, k, l, m) has been used to index reflections. While the subcell reflections vary little in their position, the satellite reflections, notably 0,2,0,−2, 1,1,0,−2, 1,3,0,−3, 1,1,0,−3, 0,0,0,2, and 1,3,1,−3, vary markedly.

modulation vector lay directly along the **b*** direction, and that it could be incommensurate with respect to **b*** (see Fig. 6 and Section 3.4).

Figure 3 shows densitometer traces from Guinier films of (a) 50 mole% ZrF_4 800°C and (b) 30 mole% ZrF_4 1000°C specimens. Both traces show a second phase to be present; ReO_3-type cubic $Zr_3O_2F_8$ (labeled C) in the 50 mole% ZrF_4 800°C specimen and baddeleyite (labeled B) in the 30 mole% ZrF_4 1000°C specimen. While the parent unit cell reflections (h, k, l, m; $m = 0$) vary little between specimens the satellite reflections shift dramatically, particularly the higher order harmonics, e.g., 0,2,0,−2; 1,1,0,−2; 1,3,0,−3; 1,1,0,−3; 0,0,0,2 and 1,3,1,−3. From these films **q/b*** was accurately derived using the 0,2,0,−2; 1,1,0,−1; 1,1,0,−2; 1,3,0,−3; 2,2,0,−3, and 2,0,0,1 satellite reflections (see Section 3.4 for indexing notation). The value of **q/b*** derived from the X-ray powder data, while in complete agreement with the value obtained from electron diffraction patterns, could be determined with higher precision. A plot of **q/b*** vs temperature of synthesis is given in Fig. 4 for samples synthesized (a) in sealed platinum tubes in air and (b) in unsealed platinum tubes under an atmosphere of nitrogen.

Within the uncertainty of the calculation of **q/b*** from the refined Guinier data for each specimen, there is complete agreement

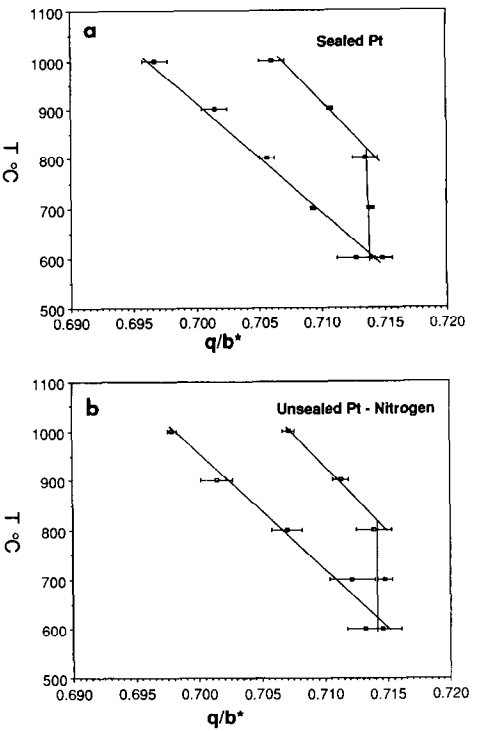

FIG. 4. Plot of XRD-determined **q/b*** versus temperature of synthesis for $ZrO_{2-x}F_{2x}$ in the two series of specimens. Within experimental uncertainty there is complete agreement between results for specimens with the same starting composition and temperature of synthesis, despite other conditions being different.

between the results for specimens with the same starting composition and temperature of synthesis, despite other conditions of synthesis being quite different. From this result we conclude that the magnitude of the modulation vector for the end member compositions is dependent only on temperature. This result is surprising given that the parent unit cell dimensions are dependent on the conditions of synthesis as discussed below.

3.3 Unit Cell Dimensions

The *C*-centered orthorhombic parent unit cell dimensions of the end members of the solid–solution field were determined using a least-squares refinement of data out to 54° 2θ for Cu$K\alpha_1$. These are presented in Fig. 5 with the data from the two series, sealed Pt tubes and unsealed Pt tubes under 1 atm N_2, on the same plots.

For all the cell dimensions of both the 30 and the 50 mole% ZrO_2 specimens there is approximate agreement between the data for each series, with the **a** and **c** dimensions in greatest agreement. The **b** dimension, which corresponds to the modulation direction, shows the greatest disagreement between the equivalent specimens from the two series.

When comparing the 30 mole% ZrF_4 data with the 50 mole% ZrF_4 data the difference in magnitude of **c** is most striking. The **c** dimension is consistently 0.25% greater in the 30 mole% ZrO_2 specimens. As a function of increasing temperature **c** increases and **a** is approximately constant for both the 30 and the 50 mole% ZrO_2 specimens, whereas **b** shows poor agreement between specimens.

It is interesting to compare the cell dimensions of specimens with the same $\mathbf{q}/\mathbf{b}^*$ as shown in Fig. 4. First, let us compare the 50 mole% ZrF_4 1000°C specimens, sealed Pt and N_2 series, with the 30 mole% ZrF_4 800°C specimens, all of which have $\mathbf{q}/\mathbf{b}^* = 0.706$. The sealed Pt series subcell dimensions agree quite well but the N_2 series dimensions do not. Second, if we compare the 600°C specimens for each series, all of which have $\mathbf{q}/\mathbf{b}^* = 0.714\ (= \frac{5}{7})$ there are quite significant differences between specimens whose wave-vector magnitude is, within error, the same.

Careful remeasurement of many of the Guinier films confirmed these results. In addition the two 600°C specimens which were reannealed for a further week in sealed Pt tubes showed no change in either $\mathbf{q}/\mathbf{b}^*$ or the parent unit cell dimensions.

From these results and the plots of $\mathbf{q}/\mathbf{b}^*$ as a function of temperature of synthesis and starting composition we considered it necessary to invoke another variable to explain the apparent lack of a one-to-one relationship between $\mathbf{q}/\mathbf{b}^*$ and unit cell dimensions. This proposed variable is anion disorder and is discussed further in Section 3.7 below.

3.4 Electron Diffraction Patterns

Figure 6 shows (a) and (b) [100], (c) [010], (d) [001], and (e) [2, 0, −1] subcell zone-axis convergent beam patterns (CBPs) typical of the $ZrO_{2-x}F_{2x}$ solid solution field. A four-index notation $(h, k, l, m) = h\mathbf{a}^* + k\mathbf{b} + l\mathbf{c}^* + m\mathbf{q}$, where $\mathbf{a}^*$, $\mathbf{b}^*$, $\mathbf{c}^*$ correspond to the cell dimensions of the reciprocal lattice of the underlying *Cmmm* parent structure (see Fig. 7) and where the primary modulation wave-vector $\mathbf{q} \approx \frac{5}{7}\mathbf{b}^*$, can be used to index any given reflection. Figure 6f shows a typical selected area electron diffraction pattern (SADP) taken close to the [001] zone-axis. In this case $\mathbf{q} \approx \frac{22}{31}\mathbf{b}^*$. In general, it is difficult to distinguish between parent and satellite reflections due to the large amplitude of the first few modulation harmonics. Notice the characteristic satellite extinction condition $F(0, k, l, m) = 0$ unless $m = 2n$ in Fig. 6b. The corresponding superspace group is $P:Cmmm:s,-1,1$ (*13*).

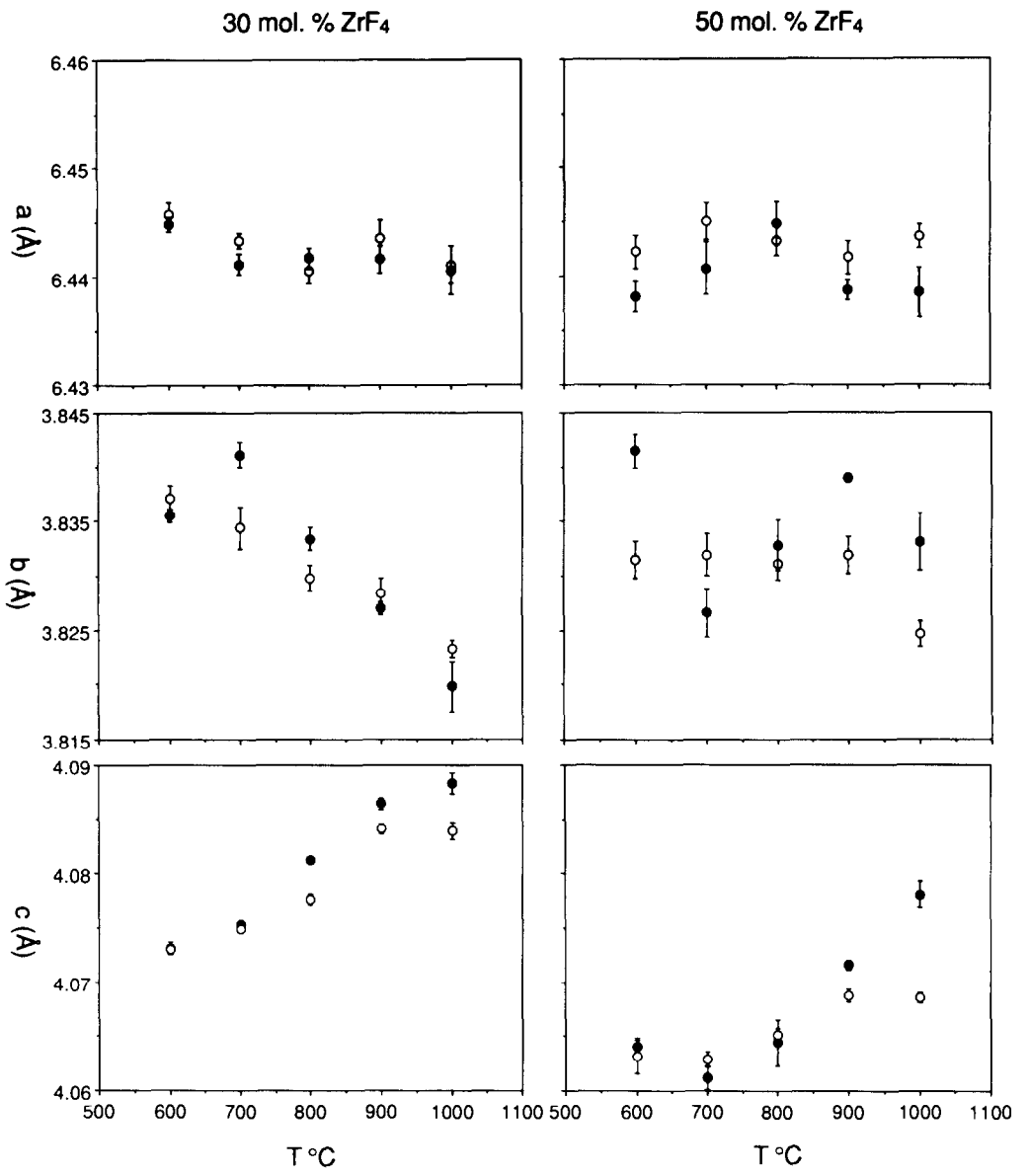

FIG. 5. Plot of refined parent unit cell dimensions versus temperature of $ZrO_{2-x}F_{2x}$ versus temperature of synthesis. Filled circles represent specimens from the sealed Pt tube series and open circles from the open (crimped) Pt tubes under 1 atm N_2 series.

Notice also the characteristic diffuse intensity present in Figs. 6a, 6c, and 6e. There seems to be three distinct types of diffuse intensity present. The first consists of diffuse sheets of intensity perpendicular to $\mathbf{c}^*$ and running through the $\mathbf{G} \pm \frac{1}{2}\mathbf{c}^*$ reciprocal space positions (horizontal arrows in Figs. 6a, 6c and 6e). The strong azimuthal intensity variation displayed by this type of diffuse distribution in wider

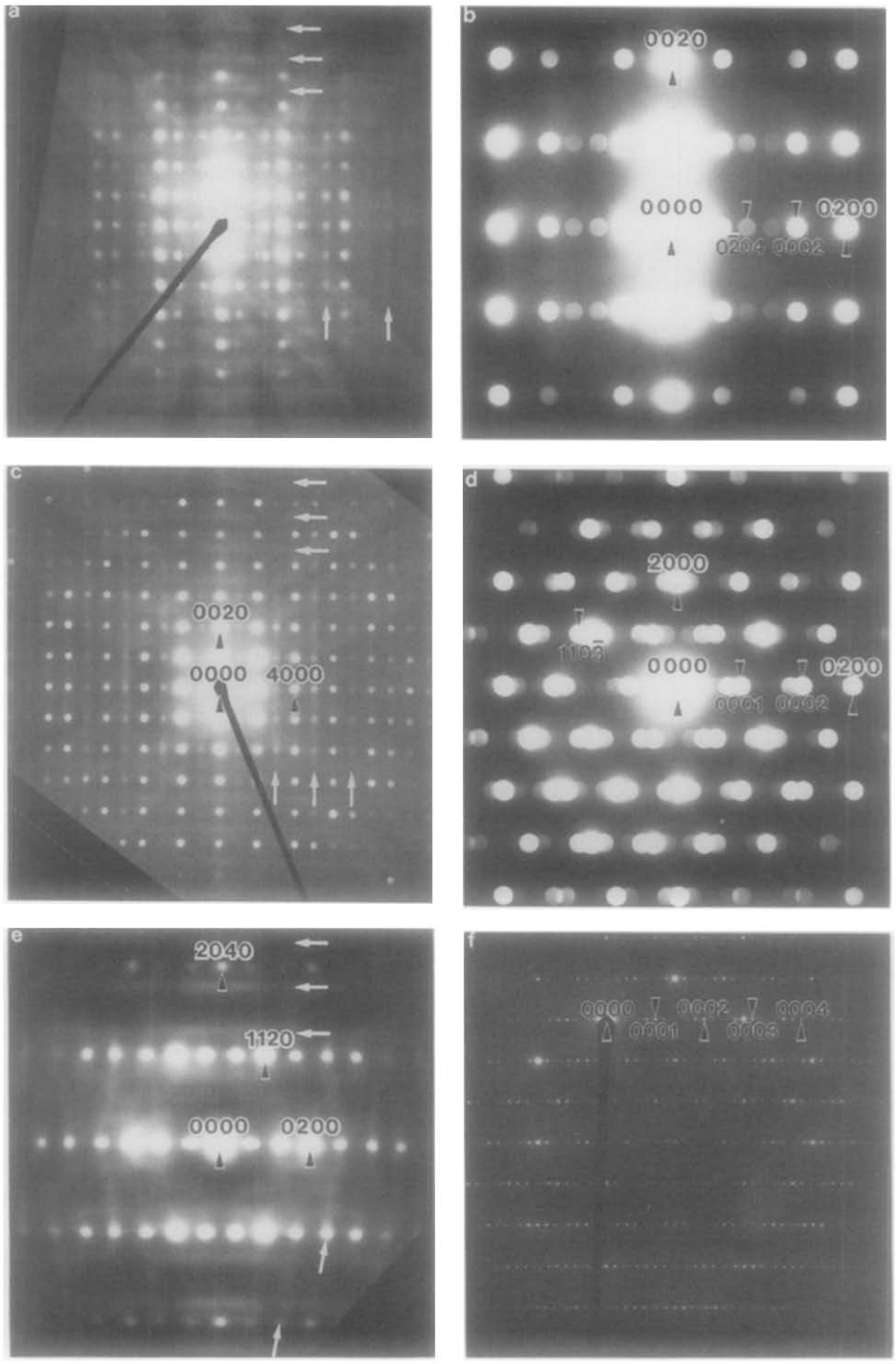

FIG. 6. Shows (a) and (b) [100], (c) [010], (d) [001], and (e) [2,0,−1] subcell zone-axis convergent beam patterns (CBPs) typical of the $ZrO_{2-x}F_{2x}$ solid solution field. Note the characteristic diffuse intensity distributions arrowed in (a), (c), and (e). A four-index notation $(h, k, l, m) = h\mathbf{a}^* + k\mathbf{b}^* + l\mathbf{c}^* + m\mathbf{q}$, where the primary modulation wave-vector, $\mathbf{q} \approx \frac{5}{7}\mathbf{b}^*$, can be used to index any given reflection. (f) Typical selected area electron diffraction pattern (SADP) taken close to the [001] zone-axis. In this case $\mathbf{q} \approx \frac{22}{31}\mathbf{b}^*$.

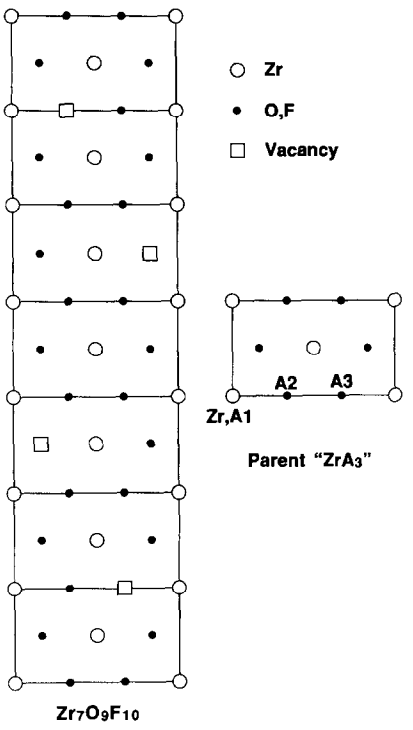

FIG. 7. The (slightly orthorhombically distorted) α-UO_3-type underlying parent structure essentially responsible for the $(h, k, l, m = 0)^*$ reflections along with the anion vacancy ordering found by Holmberg in $Zr_7O_9F_{10}$ (for $Zr_7O_9F_{10}$, Holmberg could not distinguish between O and F). The space group symmetry of the underlying parent structure is *Cmmm* ($\mathbf{a} \approx 6.44$, $\mathbf{b} \approx 3.84$, and $\mathbf{c} \approx 4.09$ Å) and there are four independent sites per primitive unit cell—Zr at 0,0,0; A_1 at $0,0,\frac{1}{2}$; A_2 at $\frac{1}{3},0,0$; and A_3 at $\frac{2}{3},0,0$.

angle [100] (Fig. 6a) and [010] (Fig. 6c) CBPs requires displacive shifts along the c axis to be responsible. This will be discussed in more detail in Section 3.7. Another weak type of diffuse consists of rods along the $\mathbf{c}^*$ direction which appear to run through the satellite, but not the parent, reflections (vertical arrows in Figs. 6a and 6c). Finally there is another type of diffuse distribution which occurs in $[h0l]$ zone-axis SADPs (sloping arrows in Fig. 6e) and is more wavy in appearance. In spite of the very sharp subcell and satellite reflections, there is clearly scope for compositional and displacive disorder.

3.5 Fourier Decomposition of the $Zr_7O_9F_{10}$ Crystal Structure

Given the continuous smooth variation of $\mathbf{q}/\mathbf{b}^*$ with composition and temperature, it is clear that any generally applicable crystallographic description of this system must be based upon a superspace group approach (*13*) rather than upon conventional crystallographic refinement at rational values of $\mathbf{q}/\mathbf{b}^*$. The underlying parent structure (see Fig. 7 and (*6*)) can be taken to be a slightly orthorhombically distorted α-UO_3-type structure. This structure is essentially responsible for the $(h, k, l, m = 0)^*$ reflections. Its space group symmetry is *Cmmm* with $\mathbf{a} \approx 6.44$, $\mathbf{b} \approx 3.84$, and $\mathbf{c} \approx 4.09$ Å. There are four independent sites per primitive parent unit cell—Zr at 0,0,0; A_1 at $0,0,\frac{1}{2}$; A_2 at $\frac{1}{3}$, 0,0; and A_3 at $\frac{2}{3},0,0$. For $Zr_7O_9F_{10}$, Holmberg could not distinguish between O and F. Hence we will simply refer to anion sites as A. The parent structure of $Zr_7O_9F_{10}$ has $\frac{6}{7}$ of an anion at each of the A_2 and A_3 sites on average, i.e., the average atomic scattering factor of the A_2 and A_3 sites, $\bar{f}_{A2} = \bar{f}_{A3} = \frac{6}{7} f_A$). On the other hand, the A_1 site is fully occupied,i.e., $\bar{f}_{A1} = f_A$.

The extinction conditions characteristic of this incommensurately modulated phase (see Fig. 6b where $F(0klm) = 0$ unless $m = 2n$) imply a superspace group symmetry of $P:Cmmm:s,-1,1$. Complete specification of such a structure consists of determining the above parent structure plus the atomic modulation functions (AMFs) (see Perez-Mato *et al.* (*14, 15*) describing the compositional fluctuations and displacive shifts away from this underlying parent structure as a function of $\mathbf{q} \cdot \mathbf{T}$, where $\mathbf{q} \approx \frac{5}{7}\mathbf{b}^*$ and $\mathbf{T} = m\mathbf{a} + n\mathbf{b} + p\mathbf{c} + q\,\frac{1}{2}(\mathbf{a} + \mathbf{b})$ (m, n, p, q all integers) labels the different cells of the parent structure. The above superspace group severely constrains the form of these AMFs.

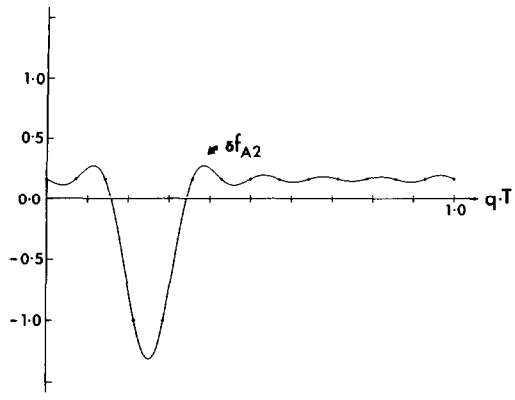

FIG. 8. Plot of the compositional AMF characteristic of the A_2 site (δf_{A2}) of $Zr_7O_9F_{10}$ (obtained by fourier decomposition of the reported crystal structure) as a function of $\mathbf{q} \cdot \mathbf{T}$.

Fourier decomposition of the reported crystal structure of $Zr_7O_9F_{10}$ enables specific expressions for these AMFs to be derived. In the case of compositional fluctuations, it is clear that these can only occur on the A_2, A_3 sites. We have $f_{A2}(\mathbf{q} \cdot \mathbf{T}) = \frac{6}{7} f_A (1 + \delta f_{A2}(\mathbf{q} \cdot \mathbf{T}))$.

Fourier decomposition of Holmberg's refinement gives:

$$\begin{aligned}\delta f_{A2}(\mathbf{q} \cdot \mathbf{T}) = &-0.3250 \cos(2\pi\, \mathbf{q} \cdot \mathbf{T} - \pi/2) \\ &- 0.3003 \cos(4\pi\, \mathbf{q} \cdot \mathbf{T} - \pi) \\ &-0.2606 \cos(6\pi\, \mathbf{q} \cdot \mathbf{T} - 3\pi/2) \\ &- 0.2078 \cos(8\pi\, \mathbf{q} \cdot \mathbf{T} - 2\pi) \\ &-0.1446 \cos(10\pi\, \mathbf{q} \cdot \mathbf{T} - 5\pi/2) \\ &- 0.0742 \cos(12\pi\, \mathbf{q} \cdot \mathbf{T} - 3\pi).\end{aligned}$$

Note that $\delta f_{A3}(\mathbf{q} \cdot \mathbf{T}) = \delta f_{A2}(\mathbf{q} \cdot \mathbf{T} + \frac{1}{2})$. This function is shown plotted as a function of $\mathbf{q} \cdot \mathbf{T}$ in Fig. 8. In the case of $Zr_7O_9F_{10}$ $\mathbf{q} = \frac{5}{7}\mathbf{b}^*$ exactly and hence this compositional modulation function is sampled at a limited number of discrete values of $\mathbf{q} \cdot \mathbf{T}$. For a general x, however, all possible values of $\mathbf{q} \cdot \mathbf{T}$ will be sampled. It is clearly strongly anharmonic as can be seen from the above expression. Note that when $\delta f_{A2}(\mathbf{q} \cdot \mathbf{T}) = \frac{1}{6}$, the corresponding site is fully occupied whereas when $\delta f_{A2}(\mathbf{q} \cdot \mathbf{T}) = -1$, the corresponding site becomes vacant.

Presumably such a modulation function would not vary too much with $\mathbf{q}$. To confirm this, however, would require full 4-D X-ray structure refinements at a range of q-values. Figures 9 and 10 also show the corresponding displacive AMFs for the Zr, A_1 and A_2 sites along both the **a** and **b** directions, respectively, (c-axis shifts are forbidden by the superspace group) as a function of $\mathbf{q} \cdot \mathbf{T}$. The ordinate is in fractional coordinates. The AMFs for the A_3 site are related to those for the A_2 site as follows:

$$U^x_{A3}(\mathbf{q} \cdot \mathbf{T}) = -U^x_{A2}(\mathbf{q} \cdot \mathbf{T} + \tfrac{1}{2})$$

$$U^y_{A3}(\mathbf{q} \cdot \mathbf{T}) = U^y_{A2}(\mathbf{q} \cdot \mathbf{T} + \tfrac{1}{2}).$$

In the case of A_2 and A_3 sites, there is some ambiguity in that there are seven allowed variables but only six equations to fit (the missing equation results from the vacant sites). We have fixed this unspecified degree

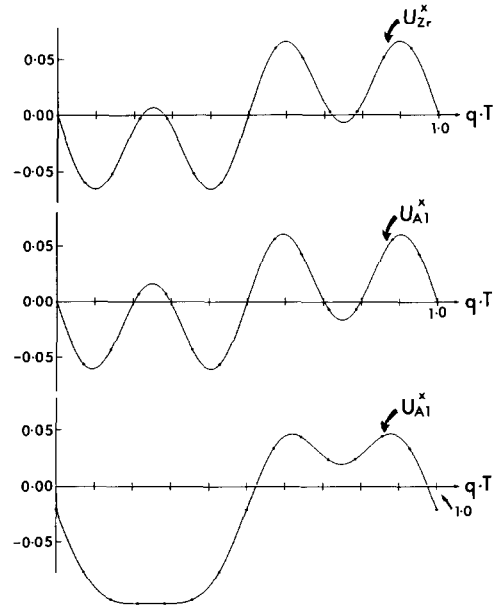

FIG. 9. Plots of the displacive AMFs along the **a** direction of the Zr, A_1, and A_2 sites of $Zr_7O_9F_{10}$ (obtained by fourier decomposition of the reported crystal structure) as a function of $\mathbf{q} \cdot \mathbf{T}$. The ordinate is in units of fractional coordinates.

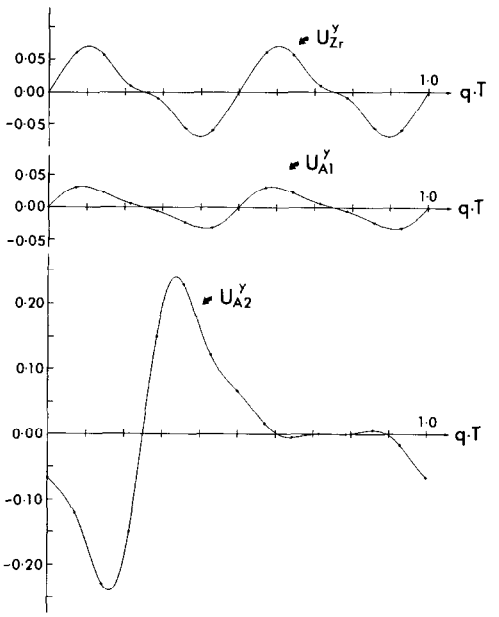

FIG. 10. Plots of the displacive AMFs along the **b** direction of the Zr, A_1, and A_2 sites of $Zr_7O_9F_{10}$ (obtained by fourier decomposition of the reported crystal structure) as a function of $\mathbf{q} \cdot \mathbf{T}$. The ordinate is in units of fractional coordinates.

of freedom such that the amplitude of the highest order harmonic allowed goes to zero. Such a choice is required by the observed diffraction patterns (see Figs. 6b and 6d).

3.6 Apparent Valence Calculations on $Zr_7O_9F_{10}$ Crystal Structure

The structure refinement of $Zr_7O_9F_{10}$ from single crystal X-ray data by Holmberg (*6*) gave quite reasonable Zr–(O, F) bond lengths and coordination polyhedra, and the anion–anion distances were also plausible. However, due to the similar X-ray scattering curves of O and F, being neighboring elements, this worker was not able to determine whether O and F atoms were ordered or disordered on each of the 10 anion sites.

By the calculation of apparent valences (AVs) (*16, 17*) for this reported structure it is possible to identify those anion sites which are occupied by O, those occupied by F, and those sites occupied by a mixture of O and F. Table I presents the AVs for all atoms in the refined structure. By considering initially the AVs of the anions, it is obvious which anion environments provide satisfactory bonding for oxygen ($X(1)$, $X(2)$, and $X(6)$), those for fluorine ($X(3)$, $X(4)$, and $X(5)$), and those which are midway ($X(7)$–$X(10)$). Once these sites are assigned (Model 1 in Table I), the AVs for all the Zr atoms become plausible, with the possible exception of Zr(1) and O(3), which are slightly overbonded. The AV for O(3) can be improved by constraining the A_1 sites ($X(7)$–$X(10)$) to be $(O_{0.5}F_{0.5})$ and O(3) to be $(O_{0.75}F_{0.25})$, which together satisfy the stoichiometry $Zr_7O_9F_{10}$ (Model 2).

In terms of the structure, it is evident from either Models 1 or 2 that there is ordering of O and F in the plane of the Zr, A_2, and A_3 layers and apparent disorder of O and F on the 2-coordinate A_1 sites between the Zr layers.

The observed **c** dimension for the $Zr_7O_9F_{10}$ structure, and indeed the entire solid solution (see Fig. 4), can also be understood in terms of AVs of atoms bonded in this direction. If we assume 50% O and 50% F occupying the interlayer 2-coordinate sites, (O, F), and impose exact ordering along the –Zr–(O, F)–Zr–(O, F)– chains parallel to **c**, we would have –Zr–F–Zr–O–Zr–F–Zr–O–. If we then constrain the AVs of these 2-coordinate F and O atoms to equal 1 and 2, respectively, then d_{Zr-F} = 2.11 Å and d_{Zr-O} = 1.94 Å. This gives d_{O-F} = 4.05 Å, in remarkable agreement with the observed **c** dimension of 4.07 Å. Note that a pure –Zr–F–Zr–F– chain would give d_{F-F} = 4.22 Å and pure –Zr–O–Zr–O– chain would give d_{O-O} = 3.87 Å. Of course, such anion ordering would imply a doubling of the *c*-axis. We believe that the experimentally observed sheets of diffuse intensity at $\frac{1}{2}\mathbf{c}^*$ in diffrac-

TABLE I

APPARENT VALENCES FOR $Zr_7O_9F_{10}$[a]

Atom	AV			Atom	AV	
	All O	All F	(O_9F_{10})[b]		Model 1[c]	Model 2[d]
Zr(1)	4.41	3.52	3.91	Zr(1)	4.23	4.25
Zr(2)	4.41	3.52	3.91	Zr(2)	4.01	4.03
Zr(3)	4.52	3.61	4.01	Zr(3)	4.00	3.98
Zr(4)	4.43	3.54	3.93	Zr(4)	3.99	3.92
O,F(1)	1.97	1.58	1.75	O(1)	1.97	1.97
O,F(2)	1.96	1.56	1.74	O(2)	1.96	1.96
O,F(3)	1.33	1.06	1.18	F(1)	1.06	1.06
O,F(4)	1.34	1.07	1.19	F(2)	1.07	1.07
O,F(5)	1.40	1.12	1.24	F(3)	1.12	1.12
O,F(6)	2.24	1.79	1.99	O(3)	2.24	2.11[d]
O,F(7)	1.53	1.23	1.36	O,F(1)	1.35	1.37
O,F(8)	1.51	1.21	1.34	O,F(2)	1.33	1.36
O,F(9)	1.53	1.22	1.36	O,F(3)	1.35	1.37
O,F(10)	1.52	1.21	1.35	O,F(4)	1.34	1.36

[a] R_0 Zr–O = 1.937 Å and R_0 Zr–F = 1.854 Å.
[b] R_0 Zr–(O, F) = 1.893 Å as (O, F) is $\frac{10}{19}$F and $\frac{9}{19}$O.
[c] R_0 Zr–(O, F) = 1.890 Å as (O, F) is $\frac{4}{7}$F and $\frac{3}{7}$O.
[d] R_0 Zr–(O, F) = 1.896 Å as (O, F) is $\frac{1}{2}$ F and $\frac{1}{2}$ O. Note that R_0 Zr–O(3) = 1.916 Å as O(3) is deemed to be $\frac{1}{4}$F and $\frac{3}{4}$O to give overall stoichiometry $Zr_7O_9F_{10}$.

tion patterns (Figs. 6a, 6c, and 6e) do indeed correspond to such ordering along –Zr–anion–Zr–anion– chains in the **c** direction. This is discussed in more detail in Section 3.7 below.

3.7 Interpretation of Diffuse Intensity Distribution

As discussed in Section 3.6 the structure refinement of $Zr_7O_9F_{10}$ (*6*) did not distinguish between O and F on the anion sites. AV calculations indicate the probable ordering of O and F on the A_2 and A_3 sites but that, in terms of the refined commensurately modulated structure, there is an equal probability of O and F on a given A_1 site.

The diffuse sheets of intensity perpendicular to **c*** and running through the $\mathbf{G} \pm \frac{1}{2}\mathbf{c}^*$ reciprocal space positions, with their strong azimuthal intensity variation (horizontal arrows in Figs. 6a, 6c, and 6e), are interpreted as due to exact –Zr–F–Zr–O– ordering in any –Zr–(O, F)–Zr–(O, F)– chain parallel to **c**. The reason why we observe sheets of diffuse and not "superstructure" reflections at $\frac{1}{2}\mathbf{c}^*$ is that the –Zr–F–Zr–O– ordering is not correlated from one chain to the next. Also, following from the AV argument concerning the required d_{Zr-F} and d_{Zr-O} in these chains, this ordering would have the effect of displacing the Zr atoms by ~0.085 Å along the **c** direction, which is consistent with the observed azimuthal intensity variation.

The diffuse rods along the **c*** direction appear to run through satellite reflections (vertical arrows in Figs. 6a and 6c) but apparently not through subcell reflections. This suggests some sort of disordering or lack of correlation in the phasing of the AMFs from one layer (normal to the **c*** direction) to the next. It is difficult, however, to be more specific. The third type of dif-

TABLE II

MODELS OF $ZrO_{2-x}F_{2x}$ ($0.0 \leq x \leq 1.0$) BASED ON α-UO_3-TYPE PARENT STRUCTURE WITH DISTANCES (Å) CONSTRAINED TO SATISFY THE VALENCE REQUIREMENTS OF Zr AND A_1

Formula:	$Zr_3O_3F_6$	$Zr_3O_3F_6$	$Zr_7O_9F_{10}$[a]	$Zr_3O_4F_4$	$Zr_3O_5F_2$	$Zr_3O_6F_0$	m-ZrO_2[b]
x	1	1	$\frac{5}{7}$	$\frac{2}{3}$	$\frac{1}{3}$	0	
A_1	O	$O_{1/2}F_{1/2}$	$O_{1/2}F_{1/2}$	$O_{1/2}F_{1/2}$	O	O	
A_2, A_3	F	$O_{1/4}F_{3/4}$	$O_{3/7}F_{4/7}$	$O_{1/2}F_{1/2}$	$O_{1/2}F_{1/2}$	O	
$d_{(Zr-A1)}$	1.94	2.03	2.03	2.03	1.94	1.94	
Coordination	2 + 6	2 + 6	2 + $5\frac{1}{7}$	2 + 5	2 + 4	2 + 3	7
$d_{(Zr-A2,A3)}$	2.26	2.20	2.13(10)[c]	2.15	2.15	2.09	2.16(8)[c]
AV (F)	1.00	1.18	—	1.34	1.34	—	
AV (O)	2.00	1.48	—	1.68	1.68	2.00	
$d_{(A-A)}$[e]	2.26	2.20	2.51[d]	2.53	3.04	3.62	2.58[d]
Vol. (Å^3)	51.4	50.9	50.3	48.7	46.6	43.9	35.6

[a] Observed $Zr_7O_9F_{10}$ structure (*6*).
[b] Observed baddeleyite structure (*12*).
[c] Mean observed $d_{(Zr-anion)}$ with standard deviation.
[d] Shortest observed $d_{(O-O)}$.
[e] Distance upon relaxation about a circle of radius $d_{(Zr-A2,A3)}$.

fuse, while similar to the above-mentioned rods in that it appears to run through satellite reflections only (Fig. 6e), is less easily interpreted because it occurs along relatively minor directions of reciprocal space.

In Section 3.3 it was considered necessary to invoke anion disorder to explain the apparent lack of one-to-one relationship between **q**/**b*** and unit cell dimensions. Given the clear electron diffraction evidence that disorder is endemic in this material it is not unreasonable to conclude that conditions of synthesis would have a significant effect on the degree of disorder. While the magnitude of the modulation wave-vector is determined by the composition of any given specimen (see Section 3.8), the unit cell dimensions are also dependent on the degree of disorder. Attempts to observe differences between specimens in the diffuse intensity distribution as a measure of disorder by electron diffraction, however, proved inconclusive.

3.8 Relationship of $q = q/b^*$ to Composition

In his discussion of series $(MA)_{2(3n+1)}A_{4(3n+1)-2n}$ Holmberg (*6*) derived the "multiplicity" of the parent structure for these phases as being $(3n + 1)\mathbf{b}$, n being an integer. Our superspace group approach to describing the solid-solution $ZrO_{2-x}F_{2x}$: $0.698 \leq x \leq 0.714$ allows a single description for all observed compositions, thereby circumventing the problem of n having to be an integer in Holmberg's series and the consequent need for invoking unit-cell scale intergrowths or "chemical twinning."

As discussed in Section 3.5, we treat the underlying parent structure as α-UO_3-type. For a given composition of $ZrO_{2-x}F_{2x}$ the average structure has $(1 - x)/2$ of an anion at each of the A_2 and A_3 sites, i.e., the probability of an anion vacancy on the A_2 and A_3 sites in the "ideal" ZrA_3 parent structure is $\frac{1}{2}(1 - x)$. This does not, however, of itself fix q. Reasonable physical constraints need to be imposed in order to do this. The constrains we have imposed is that the **b**-component of anion vacancy separation must never be less than $\frac{3}{2}\mathbf{b}$ and never greater than $\frac{4}{2}\mathbf{b}$ (in order to relieve anion crowding—see Section 3.9 below). Under the assumption of an idealized square wave compositional modulation function, such a constraint requires q to

equal either x or $(1 - x)$. Experimentally, however, it is clear that $q = x$ rather than $(1 - x)$ (see the SADP in Fig. 6f). An additional constraint which would force this result is that vacancies separated by $\frac{3}{2}\mathbf{b}$ must belong to the same string type, i.e., to either an A_2 or an A_3 string but not one to each. Both these constraints are obeyed by the refined structure ($x = \frac{5}{7}$) $Zr_7O_9F_{10}$ (*6*). Thus we believe that stoichiometry and primary modulation wave-vector are directly related via the formula $\mathbf{q}/\mathbf{b}^* = x$.

3.9 Why $x \approx \frac{5}{7}$ in $ZrO_{2-x}F_{2x}$

In this section we attempt to broadly explain why $x \approx \frac{5}{7}$ in $ZrO_{2-x}F_{2x}$, why this compound possesses such a narrow composition range ($0.698 \leq x \leq 0.714$), and why the composition range shifts to lower values of x with increasing temperature of synthesis.

In the α-UO_3-type parent structure the only significant nonbonding atomic interaction is between A_2 and A_3. If we consider this interaction as a function of composition for selected values of x across the composition range, while exactly satisfying the bond valence requirements for the atoms Zr and A_1, it becomes clear why a composition in the vicinity of $x = \frac{2}{3}$ provides the necessary compromise between first and second neighbor interactions. Table II lists the various calculated parameters of five hypothetical structures as well as equivalent observed parameters for $Zr_7O_9F_{10}$ (*6*) and baddeleyite (m-ZrO_2).

Let us first consider the two extremes of composition ($x = 1.0$ and $x = 0.0$) where valence requirements can be satisfied exactly by ordering of anions or vacancies. It is immediately apparent that $ZrOF_2$ could not adopt this structure as a $d_{(A-A)}$ around the perimeter of the hexagonal bipyramid would be too short, even for fluorine. While $d_{(A-A)}$ is not a problem for α-UO_3-type ZrO_2 this structure is necessarily unstable with respect to the observed 1 atm room temperature structure, namely baddeleyite. The volume of α-UO_3-type ZrO_2 (CN = 2 + 3) is some 23% greater than that of baddeleyite (CN = 7).

It follows that, as x decreases, α-UO_3-type $ZrO_{2-x}F_{2x}$ will become stable when there is no longer anion crowding about the perimeter of the Zr polyhedron. For the $x = \frac{2}{3}$ model, equivalent to the α-U_3O_8-type, where the anions relax to form a pentagonal bipyramid, $d_{(A-A)}$ increases to an acceptable 2.53 Å. As x decreases further this distance progressively increases, suggesting that α-UO_3-type $ZrO_{2-x}F_{2x}$ would become unstable with respect to the efficiently packed $x \approx \frac{2}{3}$ model and baddeleyite. That the region of stability occurs at $x \approx \frac{5}{7}$ and not at $x = \frac{2}{3}$ highlights the crudity of this explanation and the gross simplifications made in these calculations. For example, neither regular pentagonal bipyramids (CN 2 + 5) nor octahedra (CN 2 + 4) can be packed together regularly in a manner consistent with an α-UO_3-type parent. Nevertheless, by attempting to satisfy both first neighbor (bond valence) and second neighbor (anion packing) requirements we arrive at a theoretical composition for $ZrO_{2-x}F_{2x}$ in moderate agreement with our observations.

When we consider the $d_{(A-A)}$'s in the $Zr_7O_9F_{10}$ structure, which corresponds to the highest experimentally observed value for x (Fig. 4), we see that, along the chains of anions in the modulation direction **b**, the anions are indeed in "contact" (Table III). The shortest $d_{(O-O)}$ is 2.51 Å, which compares with 2.58 Å in baddeleyite and 2.57 Å in α-U_3O_8 (*18*).

To explain why the composition range is so narrow one can only suggest that the balance between anion "overcrowding" and "undercrowding" must be very delicate. This explanation, though trite, is supported by the observation that, above 800°C, the range is apparently constant while shifting to lower x with increasing

TABLE III

ANION–ANION DISTANCES (Å) IN $Zr_7O_8F_{10}$ (*6*) AND α-U_3O_8* (*18*) ALONG THE MODULATION DIRECTION **b**

$Zr_7O_9F_{10}$		α-U_3O_8	
F(3)		O(5)	
	2.45		2.57
O(3)		O(3)	
	2.45		2.57
F(2)		O(5)	
	2.43		2.57
O(2)		O(4)	
	2.51		3.02
O(1)		O(4)	
	2.55		2.57
F(1)		O(5)	
	2.50		
F(3)			

temperature. Given that the upper limit of x is determined by the closest anion–anion contacts it is, therefore, not surprising that x decreases with increasing temperature of synthesis, as this affords an increase in the $d_{(A-A)}$'s required by the higher temperature structures.

4. Conclusion

It is evident from this study that $ZrO_{2-x}F_{2x}$: $0.698 \leq x \leq 0.714$ is best described as a single incommensurately modulated structure with primary modulation wave vector varying with composition. The XRD and electron diffraction observations that the magnitude of the wave vector varies continuously across the composition range precludes any description which requires a limited number of "line phases" to be intergrown on the unit cell scale. It is, however, understandable that previous authors attempted such descriptions in the absence of the now acceptable alternative we have at our disposal, namely, the incommensurately modulated structure.

Our endeavours to explain in broad crystal chemical terms why this compound is stable in the vicinity of $x = \frac{2}{3}$ and over such a narrow composition range, while plausible, do emphasize the need for very accurate four-dimensional crystal structure refinements of such compounds. In the case of $ZrO_{2-x}F_{2x}$, it is essential to resolve O, F ordering. The present authors are currently undertaking such refinements of this rather anharmonically modulated structure for a range of values of x toward a better understanding of this fascinating material.

Acknowledgments

The authors express their gratitude to Professor B.G. Hyde for fruitful discussions, to Mr. K. Owen for assistance with the densitometer traces, and to Mr. P. Barlow for assistance with the illustrations.

References

1. B. GAUDREAU, *Rev. Chim. Miner.* **2,** 1 (1965).
2. P. JOUBERT AND B. GAUDREAU, *Rev. Chim. Miner.* **12,** 289 (1975).
3. R. PAPIERNIK, "Synthesis and Structural Characterisation of Some Oxyfluorides of Zirconium and Uranium," Thesis, University of Limoges (1984).
4. R. PAPIERNIK, B. FRIT, AND B. GAUDREAU, *Rev. Chim. Miner.* **23,** 400 (1986).
5. R. PAPIERNIK AND B. FRIT, *Acta Crystallogr. Sect. B* **42,** 342 (1986).
6. B. HOLMBERG, *Acta Crystallogr. Sect. B* **26,** 830 (1970).
7. R. PAPIERNIK AND B. FRIT, *Mater. Res. Bull.* **19,** 509 (1984).
8. R. PAPIERNIK AND B. FRIT, *Rev. Chim. Miner.* **21,** 321 (1984).
9. A. ATKINSON, K. NELSON, AND T. M. VALENTINE, *Radioactive Waste Manage. Nucl. Fuel Cycle* **5,** 345 (1984).
10. J. G. THOMPSON, R. L. WITHERS, J. SELLAR, P. J. BARLOW, AND B. G. HYDE, *J. Solid State Chem.* **88,** 465 (1990).
11. R. S. ROTH, J. L. WARING, W. S. BROWER, AND H. S. PARKER, *in* "Solid State Chemistry: Proc. 5th. Mater. Res. Symp." (R. S. Roth and S. J. Schneider, Eds.), NBS Special Publ. 364, p. 183 (1972).
12. D. K. SMITH AND H. W. NEWKIRK, *Acta Crystallogr.* **18,** 983 (1965).
13. P. M. DE WOLFF, T. JANSSEN, AND A. JANNER, *Acta Crystallogr. Sect. A* **37,** 625 (1981).

14. J. M. PEREZ-MATO, G. MADARIAGA, AND M. J. TELLO, *J. Phys C: Sol. State Phys.* **19,** 2613 (1986).
15. J. M. PEREZ-MATO, G. MADARIAGA, F. J. ZUNIGA, AND A. GARCIA ARRIBAS, *Acta Crystallogr. Sect. A* **43,** 216 (1987).
16. I. D. BROWN AND D. ALTERMATT, *Acta Crystallogr. Sect. B* **41,** 244 (1985).
17. M. O'KEEFFE, *Struct. Bonding* **71,** 161 (1989).
18. B. O. LOOPSTRA, *Acta Crystallogr.* **17,** 651 (1964).